NANO LETTERS

pubs.acs.org/NanoLett Letter

Imaging Quantum Interference in Stadium-Shaped Monolayer and Bilayer Graphene Quantum Dots

Zhehao Ge,[▽] Dillon Wong,[▽] Juwon Lee, Frederic Joucken, Eberth A. Quezada-Lopez, Salman Kahn, Hsin-Zon Tsai, Takashi Taniguchi, Kenji Watanabe, Feng Wang, Alex Zettl, Michael F. Crommie,* and Jairo Velasco, Jr.*

Cite This: *Nano Lett.* 2021, 21, 8993−8998 Read Online

ACCESS | Metrics & More | Article Recommendations | Supporting Information

ABSTRACT: Experimental realizations of graphene-based stadium-shaped quantum dots (QDs) have been few and have been incompatible with scanned probe microscopy. Yet, the direct visualization of electronic states within these QDs is crucial for determining the existence of quantum chaos in these systems. We report the fabrication and characterization of electrostatically defined stadium-shaped QDs in heterostructure devices composed of monolayer graphene (MLG) and bilayer graphene (BLG). To realize a stadium-shaped QD, we utilized the tip of a scanning tunneling microscope to charge defects in a supporting hexagonal boron nitride flake. The stadium states visualized are consistent with tight-binding-based simulations but lack clear quantum chaos signatures. The absence of quantum chaos features in MLG-based stadium QDs is attributed to the leaky nature of the confinement potential due to Klein tunneling. In contrast, for BLG-based stadium QDs (which have stronger confinement) quantum chaos is precluded by the smooth confinement potential which reduces interference and mixing between states.

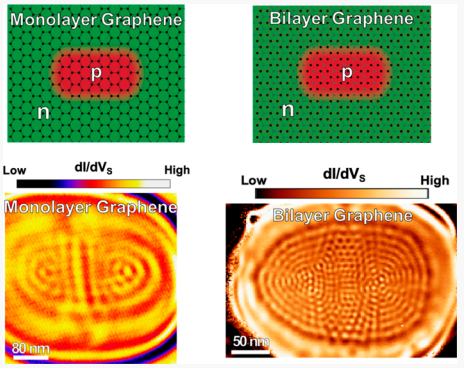

KEYWORDS: *Quantum dots, Monolayer graphene, Bilayer graphene, Quantum chaos, STM*

The advent of pristine, exposed circular p−n junctions in monolayer graphene (MLG)[1] and Bernal-stacked bilayer graphene (BLG)[2] has enabled the realization of electrostatically defined quantum dots (QDs) that are accessible to atomically resolved scanning probe microscopy. The charge carriers of these QDs possess chirality, and so their electronic states are exotic and are unlike the states in conventional semiconductor QDs.[3−5] For example, recent scanning tunneling microscopy (STM) studies of electrostatically defined MLG and BLG QDs have revealed relativistic quasi-bound states,[6,7] correlated states manifesting a wedding-cake-like charge density,[8] and states with broken rotational symmetry and nontrivial band topology.[9] So far, the QD systems studied using this technique have all been based on circularly-symmetric boundaries.[6,8−10]

Other QD symmetries, however, are possible and create new opportunities to observe novel behavior. For example, electron transport studies of conventional semiconductor-based QDs have demonstrated that circular- and square-shaped QDs host regular dynamics, while stadium-shaped QDs are described by chaotic quantum billiards.[11−14] This is the quantum mechanical analogue to the Bunimovich billiard (also known as the stadium billiard), a well-known classical chaotic system.[15] Chaotic behavior here is attributed to the nonintegrability of the classical dynamics in a stadium billiard: i.e., the existence of open orbits. Novel electronic states are expected to result from the quantum mechanical behavior of such classically chaotic systems. An example is scarred wave functions, which are characterized by standing waves that follow semiclassical periodic orbits.[13] Extensive theoretical analysis has been performed on scarred wave functions,[13,16] and numerous experimental studies have imaged analogous phenomena in surface water waves,[17] ultrasonic acoustic fields,[18] microwave cavities,[19,20] and soap films.[21] A number of predictions for scarred wave functions in graphene-based systems have also been made,[22,23] but no direct visualization of electronic states in electrostatically defined nonintegrable MLG or BLG QDs has yet been reported.

Here we report the fabrication and imaging of electrostatically defined MLG and BLG QDs that are nonintegrable. The QDs were fabricated using an STM-based technique whereby electrostatic charge is injected directly into the hexagonal boron nitride (hBN) insulating layer underlying our graphene samples. QDs with stadium-shaped boundaries were synthe-

Received: June 11, 2021
Revised: October 16, 2021
Published: October 26, 2021

https://doi.org/10.1021/acs.nanolett.1c02271
Nano Lett. 2021, 21, 8993−8998

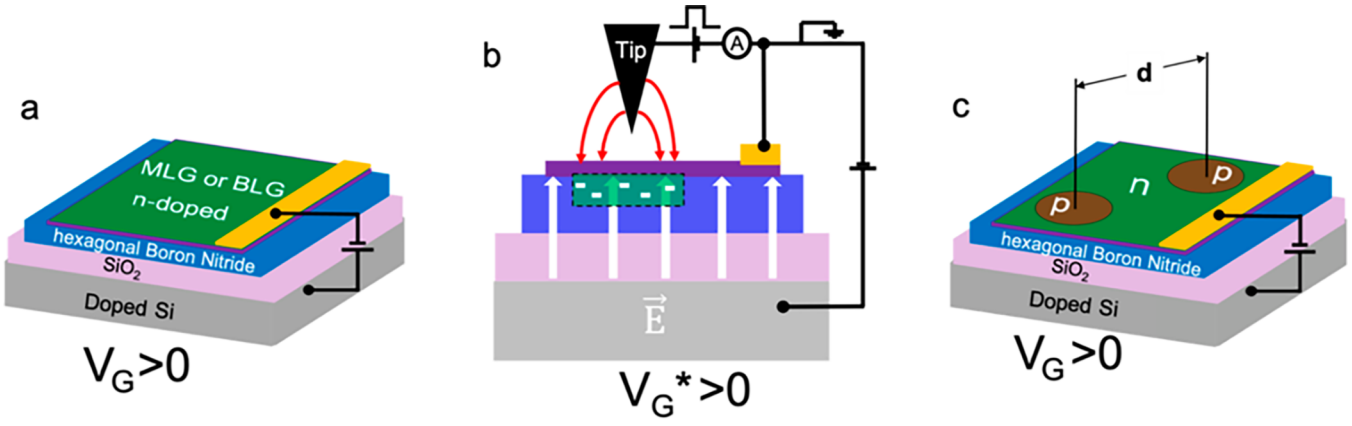

Figure 1. Schematic for creating noncircular quantum dots (QDs) on monolayer graphene (MLG) or bilayer graphene (BLG) on hexagonal boron nitride (hBN). (a) MLG or BLG/hBN heterostructure supported by an SiO_2/Si substrate. The graphene layer is contacted by gold electrodes, and a backgate voltage V_G is applied to the doped Si substrate. (b) To fabricate multiple p−n junctions, voltage pulses are applied to the scanning tunneling microscope (STM) tip at two different locations on the MLG or BLG sample while holding $V_G^* > 0$. (c) Spatial control of the resulting p−n junction (i.e., QD) geometry is achieved by applying voltage pulses at different locations separated by the distance d.

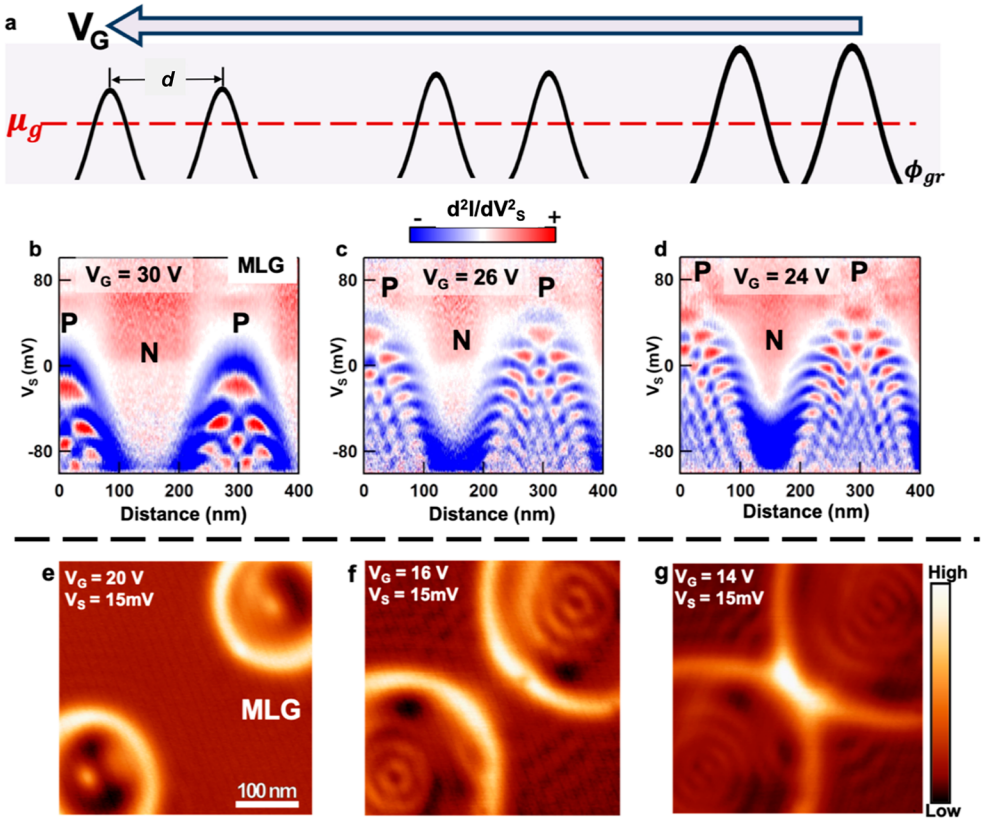

Figure 2. Control and visualization of gate-tunable quantum dots in MLG. (a) Sketch showing how modulation of V_G allows the QD electrostatic potential to be shifted with respect to the MLG chemical potential, μ_g. (b) d^2I/dV_S^2 measured as a function of sample bias (V_S) and distance from the center of one QD to the outer edge of a second adjacent QD (V_G = 30 V, V_S = −0.1 V, I = 1.0 nA, 1 mV ac modulation). (c, d) The same as (b), but with (c) V_G = 26 V and (d) V_G = 24 V. (e) dI/dV_S map for two MLG QDs (V_S = 15 mV, I = 0.5 nA, V_G = 20 V, 1 mV ac modulation). (f, g) dI/dV_S maps at the same location as (e), but with (f) V_G = 16 V and (g) V_G = 14 V. The bright bands (regions of high dI/dV_S) indicate the location of the QD barrier wall. As V_G is decreased, the circular p-doped graphene regions increase and merge.

sized by performing multiple tip injections to define each QD. Our STM measurements of the electronic wave functions of stadium-shaped QDs showed significant differences between MLG and BLG stadia, including interior nodal patterns and the presence of diagonal streaking, but no clear evidence of scarring phenomena was observed. Simulations of our QDs using a tight-binding-based formalism reveals that the lack of scarring for the MLG stadium arises due to Klein tunneling at the stadium boundary, whereas in BLG the main culprit is the smoothness of the QD boundary. Diagonal streaking in the BLG stadium is shown to be a signature of the nonintegrable nature of the QD boundary.

Figure 1 sketches our method for creating noncircular QDs in a MLG (or BLG)/hBN heterostructure supported by an

https://doi.org/10.1021/acs.nanolett.1c02271
Nano Lett. 2021, 21, 8993−8998

SiO_2/Si substrate. A backgate voltage (V_G) applied to the doped Si substrate permits global tuning of the MLG (or BLG) doping level (Figure 1a). Local modification of the potential is achieved by applying a 5 V pulse to the STM tip for 60 s that causes electric-field-induced excitation of defect states in hBN below the STM tip.[2,24] This liberates defect charge that drifts toward the MLG (or BLG) under the applied V_G*, thus leaving behind charged ions that locally gate the MLG (or BLG) above. It is possible to create multiple QDs by simply repeating this procedure at points separated by a distance d (Figure 1c). Additional tuning of the QD behavior is possible by subsequently modulating V_G, as shown in Figure 2a. Here the potential landscape for two QDs is represented by two bell-shaped potentials having centers spaced apart by d.[6,10,25] Increasing V_G causes a vertical shift of the potential landscape with respect to the MLG (or BLG) chemical potential (μ_g), which is shown as a dashed red line in Figure 2a. Such V_G modulation changes the width of each bell-shaped potential at μ_g, thus enabling modification of the QD size.

To experimentally characterize how the properties of adjacent QDs are modified by changing V_G, we performed spatially resolved spectroscopic mapping of QDs fabricated using the local electric-field treatment described above. Figure 2b−d shows the spectroscopic characterization of two adjacent QDs fabricated in a MLG/hBN heterostructure. d^2I/dV_S^2 is plotted as a function of sample-tip bias along a line extending from the center of one circular QD to the outer edge of the adjacent circular QD. Each panel represents a measurement performed at a different value of V_G. An outer envelope is observed (blue) along with an internal nodal structure (red and blue). As V_G is reduced, these features all shift upward with respect to V_S = 0, which corresponds to μ_g. Because these data originate from a MLG/hBN heterostructure, the observed nodal pattern corresponds to relativistic quasi-bound states similar to those previously reported for electrostatically defined MLG QDs.[6] The notable bending of these states near the QD boundary reflects the influence of the biased STM tip as discussed by Quezada-Lopéz et al.[25]

A more complete picture of the QD shape modification and electronic states is attained by acquiring dI/dV_S maps at constant sample-tip bias and different V_G values (Figure 2e−g). Each dI/dV_S map here displays two circular QDs with bright boundaries surrounded by outer regions having little dI/dV_S intensity change (the QDs shown in Figure 2e−g are different from those shown in Figure 2b−d but were acquired using a similar procedure). As the gate voltage is decreased from V_G = 20 V (Figure 2e) to V_G = 16 V (Figure 2f) the internal structure of the QDs is seen to include more concentric, circularly symmetric states. For example, in Figure 2e only one central antinode is visible, while after reducing V_G numerous ringlike states appear. The increase in the number of ringlike states indicates that higher-energy QD states are being probed. A decrease in the gate voltage is also seen to cause the diameter of each QD to increase, eventually causing the QDs to merge, as shown in Figure 2g. V_G modulation thus enables the realization of new, noncircular QDs through the merging of circular QDs.

We have exploited this technique to fabricate noncircular MLG and BLG QDs with boundary geometries similar to those of nonintegrable QDs previously studied in semiconductor heterojunctions.[11,14] This was accomplished by performing multiple tip pulses with a separation of $d \approx 100$ or $d \approx 50$ nm and then modulating V_G to further control the QD electronic states. Figure 3a,b shows constant-bias dI/dV_S maps at different V_G values for a noncircular MLG QD created using

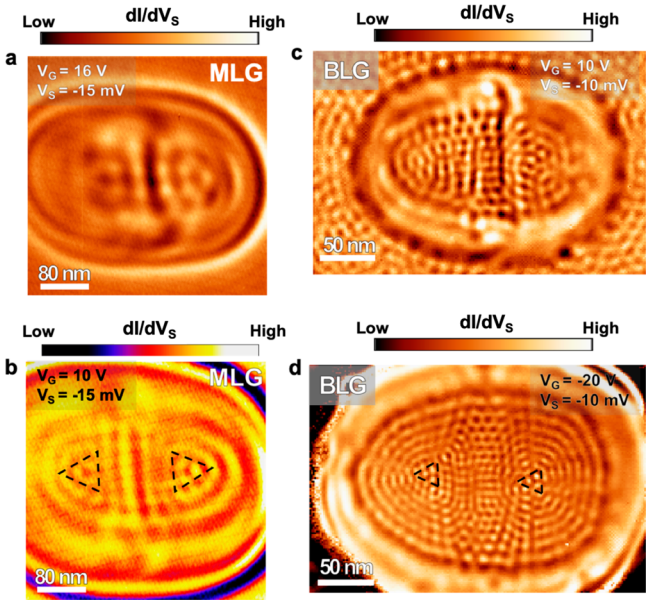

Figure 3. Visualization of gate-tunable stadium-shaped QDs in MLG and BLG sheets. (a) dI/dV_S map for a stadium-shaped MLG QD (V_S = −15 mV, I = 0.5 nA, V_G = 16 V). (b) dI/dV_S map at the same location as (a), but with V_G = 10 V. Triangles outline trigonally symmetric nodal patterns. (c) dI/dV_S map for a stadium-shaped BLG QD (V_S = −10 mV, I = 0.1 nA, V_G = 10 V). (d) dI/dV_S map at the same location as (c), but with V_G = −20 V. Triangles outline trigonally symmetric nodal patterns. As V_G is decreased, the size of the stadium-shaped QDs increases and higher-energy QD states are visualized.

this procedure. The data reveal a stadium-shaped structure with internal nodal patterns that change as the gate voltage is decreased from V_G = 16 V (Figure 3a) to V_G = 10 V (Figure 3b). Figure 3a exhibits a vertical dark stripe in the center of the stadium QD that evolves into a pattern of antinodes as V_G is reduced (Figure 3b). Additional characteristic features visible in Figure 3b are two structures having trigonal symmetry that lie in each half of the stadium (outlined by two triangles).

We similarly created stadium-shaped BLG QDs as shown in Figures 3c,d. These QDs also exhibit a vertical dark stripe at the stadium center at high gate voltage as well as trigonal patterns at the stadium ends that become visible at lower gate voltage. The trigonal patterns in the BLG QD are different from those seen in the MLG QD because the BLG patterns "point" in the same direction (see triangle outlines in Figure 3d). The BLG stadium QD also shows streaks in dI/dV_S intensity that emanate diagonally from the QD trigonal patterns and intersect with the top and bottom walls. These streaks are not seen in the MLG QD.

We now discuss the origin of the patterns in the MLG and BLG stadiums, as well as the apparent absence of scarred wave functions (more dI/dV_S maps for MLG and BLG stadia showing the absence of scarred wave functions can be found in section 5 in the Supporting Information). We first note that the dark vertical stripe seen in the central regions of both the MLG and BLG stadia can be attributed to a charge-trapping potential. This arises since the overall QD potential is created by multiple tip-pulses spaced a distance apart, and so the top of

https://doi.org/10.1021/acs.nanolett.1c02271
Nano Lett. 2021, 21, 8993−8998

the potential takes the form of two bell-shaped structures with a dip (i.e., vertical stripe) in the middle. Decreasing V_G causes the bell-shaped potentials to merge and the QD electronic state at E_F to shift from the top of the potential to a lower regime where the potential landscape is more homogeneous and where the center of the stadium exhibits a more complex nodal structure.

To further understand our experimental findings, we performed numerical tight-binding-based simulations of MLG and BLG stadium-shaped QDs. A flat-bottomed potential with smooth boundaries was used for the simulations, and we explored both the ungapped MLG electronic structure and the gapped BLG electronic structure with trigonally warped bands. These configurations are schematically depicted in Figure 4a,b,

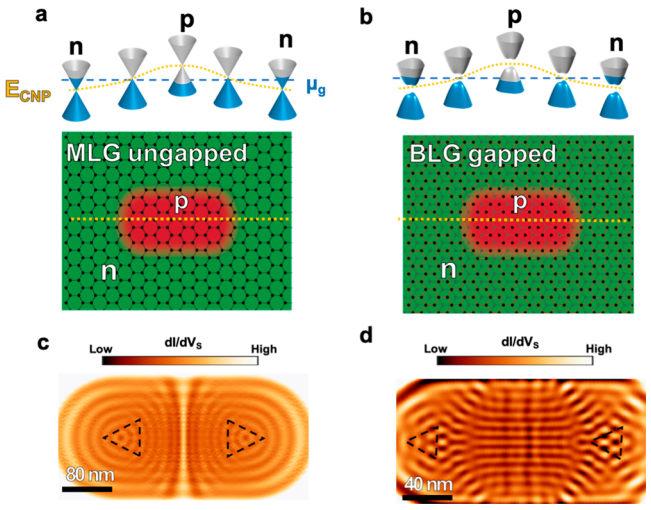

Figure 4. Stadium QD potential profile schematic and associated simulations. (a) Upper panel: MLG stadium QD potential profile schematic depicting the MLG bands and charge neutrality point (E_{CNP}) both inside and outside of the QD. Lower panel: schematic representation of stadium MLG QD. (b) Upper panel: BLG stadium QD potential profile schematic depicting the gapped and trigonally warped BLG bands and E_{CNP} inside and outside of the QD. Lower panel: Schematic representation of stadium-shaped BLG QD. (c, d) Numerical tight-binding simulations of electronic local density of states for (c) MLG and (d) BLG stadium QDs. dI/dV_S diagonal streaks are visible in (d) (which has gapped barrier walls) but not in (c) (which has ungapped walls). γ_3 hopping and a spatially uniform 60 meV gap are included in the TB model of the BLG stadium. These parameters are motivated by our previous experimental characterization of circular BLG QDs[9] (also see section 6 in the Supporting Information). The LDOS contribution from only sublattice A_1 is considered in the BLG stadium dI/dV_S map simulation.

and the resulting simulations of the stadium constant-energy dI/dV_S maps (i.e., the resulting local density of states (LDOS) patterns) are shown in Figure 4c,d. More details on the simulations can be found in section 1 in the Supporting Information. Similarities between the simulations and the experimental stadia are evident, and the role of the QD walls is also revealed by the calculations. For example, in the gapless MLG calculation of Figure 4c a 3-fold-symmetric pattern is seen on each side of the stadium (triangles) that points outward and agrees with the experimental data of Figure 3b. The simulated BLG stadium in Figure 4d displays 3-fold symmetric patterns on each side that point in the same direction (see triangles) and are similar to the data seen in Figure 3d (see section 2 in the Supporting Information for close-up plots). Figure 4d also exhibits diagonal streaks that are in qualitative agreement with the experimental dI/dV_S intensity of Figure 3d.

We are able to gain new insight into why scarred wave functions are absent in the QD stadia by examining the nature of the QD walls. For the MLG stadium, hole states inside of the QD are spatially adjacent to empty conduction-band electron states immediately outside of the stadium, thus leading to charge-carrier escape via Klein tunneling.[26] The resulting lack of strong confinement in MLG structures precludes the interference of unstable classical orbits that gives rise to scarring. This reasoning, however, suggests that scarred wave functions should be visible in a BLG stadium QD, since the nature of the walls in a BLG stadium enables stronger confinement, thus increasing the interference between unstable classical orbits. Our experimental findings for the BLG stadium QD, however, do not agree with this expectation.

To understand the absence of scarred wave functions in BLG stadium QDs, we examine key differences between the QDs realized in our experiment and previously studied systems. In our experimental BLG QDs the nature of the confinement potential is smooth, while in the initial theoretical work by Heller the confinement potential was sharp.[13] Smooth potential barriers, on the other hand, have been found to suppress quantum chaos in semiconductor-based QDs.[27] Such behavior has been attributed to dispersion in the energy of confined states at the boundaries which reduces the interference and mixing of states.[27] Stadiums with sharp potentials do not exhibit dispersion at the boundaries, thus allowing better interference and mixing of states that have similar energies and ultimately leading to wave function scarring.[13]

To further support our hypothesis that the potential well sharpness precludes us from observing scarred wave functions for a BLG stadium in experiments, we simulated LDOS maps for a stadium-shaped BLG QD with a step potential well. Consequently, we found several possible scarred wave functions (data are shown in section 7 in the Supporting Information). Video clips showing the evolution of simulated LDOS maps at different energies for a BLG stadium with a smooth potential well (in which scarred wave functions are absent) and a step potential well (in which candidate scarred wave functions are present) can also be found in the Supporting Information.

Additionally, we performed level statistical analysis for electrostatically defined MLG and BLG stadia with different potential well depths and sharpnesses (see section 9 in the Supporting Information). Level statistical analysis has been widely used to investigate the chaotic behavior of either relativistic or nonrelativistic quantum systems.[22,28] We observed a transition from Poisson level spacing distribution to Gaussian orthogonal ensemble distribution when the depth and sharpness of the potential well is increased for both MLG and BLG stadia. This finding indicates that a deeper and sharper potential well enhances the chaotic behavior of both MLG and BLG stadia. For MLG stadia, we believe the chaotic behavior is enhanced with a deep and sharp potential well because of the onset of strong intervalley scattering caused by the sharp potential well. Such intervalley scattering will suppress Klein tunneling, which is a single-valley phenomenon.

Despite the absence of wave function scarring in our BLG stadium QDs, the appearance of diagonal streaks in both the

https://doi.org/10.1021/acs.nanolett.1c02271
Nano Lett. 2021, 21, 8993−8998

experimental dI/dV_S maps and the simulated BLG QD maps provides a connection to quantum chaotic phenomenon (additional simulated dI/dV_S maps for a BLG stadium with different aspect ratios are provided in section 4 in the Supporting Information). First, the absence of diagonal streaks in integrable systems regardless of confinement strength suggests that they are a special feature of nonintegrable systems.[11,13] Second, we find that the streaks are absent in nonintegrable structures with poor confinement, such as MLG stadium QDs. This suggests that diagonal streaks require interference between states to form, similar to the phenomenon of wave function scarring.

In conclusion, we have fabricated and imaged electrostatically defined stadium-shaped QDs in MLG and BLG sheets. Our wave function maps for these QDs reveal novel features (such as diagonal streaks) that originate from fundamental differences between the electronic structures of MLG and BLG. The absence of wave function scarring in MLG stadium QDs is attributed to charge carrier escape via Klein tunneling, while for BLG stadium QDs it is attributed to the smoothness of the confinement potential. These issues can potentially be addressed by placing BLG closer to the gating source through the use of thinner hBN. Such a change in the device architecture would also sharpen the electrostatic potential,[29,30] thus potentially enabling the interference between states that is necessary for wave function scarring.

■ ASSOCIATED CONTENT

Supporting Information

The Supporting Information is available free of charge at https://pubs.acs.org/doi/10.1021/acs.nanolett.1c02271.

Evolution of simulated LDOS maps at different energies for a BLG stadium with a smooth potential well (in which scarred wave functions are absent) (AVI)

Evolution of simulated LDOS maps at different energies for a BLG stadium with a step potential well (in which candidate scarred wave functions are present) (AVI)

Numerical tight-binding calculation for electronic states within stadium-shaped MLG and BLG QDs, C_3-symmetrical patterns at the end of stadium-shaped MLG and BLG QDs, simulated dI/dV_S patterns in gapped elliptical MLG and BLG QDs, (4) simulated dI/dV_S maps for a stadium-shaped BLG QD with a different aspect ratio, additional experimental dI/dV_S maps for MLG and BLG stadia, spatially resolved band gap for the experimental BLG stadium, candidate scarred wave functions in a simulated BLG stadium with a step potential well, level statistical analysis of an experimental BLG stadium, and level statistical analysis of simulated MLG and BLG stadia (PDF)

■ AUTHOR INFORMATION

Corresponding Authors

Michael F. Crommie − *Department of Physics, University of California, Berkeley, California 94720, United States; Materials Sciences Division, Lawrence Berkeley National Laboratory, Berkeley, California 94720, United States; Kavli Energy NanoSciences Institute at the University of California, Berkeley, and the Lawrence Berkeley National Laboratory, Berkeley, California 94720, United States;* orcid.org/0000-0001-8246-3444; Email: crommie@berkeley.edu

Jairo Velasco, Jr. − *Department of Physics, University of California, Santa Cruz, California 95064, United States;* Email: jvelasc5@ucsc.edu

Authors

Zhehao Ge − *Department of Physics, University of California, Santa Cruz, California 95064, United States*

Dillon Wong − *Department of Physics, University of California, Berkeley, California 94720, United States*

Juwon Lee − *Department of Physics, University of California, Berkeley, California 94720, United States*

Frederic Joucken − *Department of Physics, University of California, Santa Cruz, California 95064, United States;* orcid.org/0000-0002-9056-0081

Eberth A. Quezada-Lopez − *Department of Physics, University of California, Santa Cruz, California 95064, United States*

Salman Kahn − *Department of Physics, University of California, Berkeley, California 94720, United States*

Hsin-Zon Tsai − *Department of Physics, University of California, Berkeley, California 94720, United States*

Takashi Taniguchi − *International Center for Materials Nanoarchitectonics, National Institute for Materials Science, Tsukuba 305-0044, Japan;* orcid.org/0000-0002-1467-3105

Kenji Watanabe − *Research Center for Functional Materials, National Institute for Materials Science, Tsukuba 305-0044, Japan;* orcid.org/0000-0003-3701-8119

Feng Wang − *Department of Physics, University of California, Berkeley, California 94720, United States; Materials Sciences Division, Lawrence Berkeley National Laboratory, Berkeley, California 94720, United States; Kavli Energy NanoSciences Institute at the University of California, Berkeley, and the Lawrence Berkeley National Laboratory, Berkeley, California 94720, United States*

Alex Zettl − *Department of Physics, University of California, Berkeley, California 94720, United States; Materials Sciences Division, Lawrence Berkeley National Laboratory, Berkeley, California 94720, United States; Kavli Energy NanoSciences Institute at the University of California, Berkeley, and the Lawrence Berkeley National Laboratory, Berkeley, California 94720, United States*

Complete contact information is available at: https://pubs.acs.org/10.1021/acs.nanolett.1c02271

Author Contributions

$^{\nabla}$Z.G. and D.W. contributed equally to this work.

Author Contributions

J.V.J., M.F.C., D.W., J.L., Z.G., and F.J. conceived the work and designed the research strategy. S.K., H.-Z.T., Z.G., and E.A.Q.-L. fabricated the samples under the supervision of A.Z. and J.V.J. K.W. and T.T. provided the hBN crystals. D.W., J.L., Z.G., F.J., and E.A.Q.-L. carried out tunneling spectroscopy measurements under the supervision of M.F.C. and J.V.J. Z.G. performed numerical tight-binding calculations and simulations with input from J.V.J. J.V.J., M.F.C., Z.G., and D.W. wrote the paper. All authors discussed the paper and commented on the manuscript.

Notes

The authors declare no competing financial interest.

https://doi.org/10.1021/acs.nanolett.1c02271
Nano Lett. 2021, 21, 8993−8998

■ ACKNOWLEDGMENTS

This research was primarily supported by the sp2 program (KC2207) (STM imaging, device design) funded by the Director, Office of Science, Office of Basic Energy Sciences, Materials Sciences and Engineering Division, of the U.S. Department of Energy under Contract No. DE-AC02-05CH11231. Support was also provided by National Science Foundation grant nos. DMR-1753367 (device fabrication, simulations, STM spectroscopy) and 1807233 (graphene growth), as well as the Army Research Office under contract W911NF-17-1-0473 (device characterization). Preparation and characterization of the BN crystals (K.W. and T.T.) was funded by the Elemental Strategy Initiative conducted by the MEXT, Japan, Grant No. JPMXP0112101001, and JSPS KAKENHI, Grant No. JP20H00354. We thank the Hummingbird Computational Cluster team at UC Santa Cruz for providing computational resources and support for the numerical tight-binding calculations performed in this work.

■ REFERENCES

(1) Velasco, J.; Ju, L.; Wong, D.; Kahn, S.; Lee, J.; Tsai, H.-Z.; Germany, C.; Wickenburg, S.; Lu, J.; Taniguchi, T.; Watanabe, K.; Zettl, A.; Wang, F.; Crommie, M. F. Nanoscale Control of Rewriteable Doping Patterns in Pristine Graphene/Boron Nitride Heterostructures. *Nano Lett.* **2016**, *16*, 1620−1625.

(2) Velasco, J.; Lee, J.; Wong, D.; Kahn, S.; Tsai, H.-Z.; Costello, J.; Umeda, T.; Taniguchi, T.; Watanabe, K.; Zettl, A.; Wang, F.; Crommie, M. F. Visualization and Control of Single-Electron Charging in Bilayer Graphene Quantum Dots. *Nano Lett.* **2018**, *18*, 5104−5110.

(3) Ihn, T.; Güttinger, J.; Molitor, F.; Schnez, S.; Schurtenberger, E.; Jacobsen, A.; Hellmüller, S.; Frey, T.; Dröscher, S.; Stampfer, C.; Ensslin, K. Graphene single-electron transistors. *Mater. Today* **2010**, *13*, 44−50.

(4) Liu, X.; Hersam, M. C. 2D materials for quantum information science. *Nature Reviews Materials* **2019**, *4*, 669−684.

(5) Matulis, A.; Peeters, F. Quasibound states of quantum dots in single and bilayer graphene. *Phys. Rev. B: Condens. Matter Mater. Phys.* **2008**, *77*, 115423.

(6) Lee, J.; Wong, D.; Velasco, J., Jr; Rodriguez-Nieva, J. F.; Kahn, S.; Tsai, H.-Z.; Taniguchi, T.; Watanabe, K.; Zettl, A.; Wang, F.; Levitov, L. S.; Crommie, M. F. Imaging electrostatically confined Dirac fermions in graphene quantum dots. *Nat. Phys.* **2016**, *12*, 1032−1036.

(7) Gutierrez, C.; Brown, L.; Kim, C.-J.; Park, J.; Pasupathy, A. N. Klein tunnelling and electron trapping in nanometre-scale graphene quantum dots. *Nat. Phys.* **2016**, *12*, 1069−1075.

(8) Gutiérrez, C.; Walkup, D.; Ghahari, F.; Lewandowski, C.; Rodriguez-Nieva, J. F.; Watanabe, K.; Taniguchi, T.; Levitov, L. S.; Zhitenev, N. B.; Stroscio, J. A. Interaction-driven quantum Hall wedding cake−like structures in graphene quantum dots. *Science* **2018**, *361*, 789.

(9) Ge, Z.; Joucken, F.; Quezada, E.; da Costa, D. R.; Davenport, J.; Giraldo, B.; Taniguchi, T.; Watanabe, K.; Kobayashi, N. P.; Low, T.; Velasco, J. Visualization and Manipulation of Bilayer Graphene Quantum Dots with Broken Rotational Symmetry and Nontrivial Topology. *Nano Lett.* **2020**, *20*, 8682−8688.

(10) Ghahari, F.; Walkup, D.; Gutiérrez, C.; Rodriguez-Nieva, J. F.; Zhao, Y.; Wyrick, J.; Natterer, F. D.; Cullen, W. G.; Watanabe, K.; Taniguchi, T.; Levitov, L. S.; Zhitenev, N. B.; Stroscio, J. A. An on/off Berry phase switch in circular graphene resonators. *Science* **2017**, *356*, 845.

(11) Marcus, C. M.; Rimberg, A. J.; Westervelt, R. M.; Hopkins, P. F.; Gossard, A. C. Conductance fluctuations and chaotic scattering in ballistic microstructures. *Phys. Rev. Lett.* **1992**, *69*, 506−509.

(12) Wilkinson, P. B.; Fromhold, T. M.; Eaves, L.; Sheard, F. W.; Miura, N.; Takamasu, T. Observation of 'scarred' wavefunctions in a quantum well with chaotic electron dynamics. *Nature* **1996**, *380*, 608−610.

(13) Heller, E. J. Bound-State Eigenfunctions of Classically Chaotic Hamiltonian Systems: Scars of Periodic Orbits. *Phys. Rev. Lett.* **1984**, *53*, 1515−1518.

(14) Chang, A. M.; Baranger, H. U.; Pfeiffer, L. N.; West, K. W. Weak Localization in Chaotic versus Nonchaotic Cavities: A Striking Difference in the Line Shape. *Phys. Rev. Lett.* **1994**, *73*, 2111−2114.

(15) Bunimovich, L. A. On the ergodic properties of nowhere dispersing billiards. *Commun. Math. Phys.* **1979**, *65*, 295−312.

(16) Jensen, R. V. Quantum chaos. *Nature* **1992**, *355*, 311−318.

(17) Blümel, R.; Davidson, I. H.; Reinhardt, W. P.; Lin, H.; Sharnoff, M. Quasilinear ridge structures in water surface waves. *Phys. Rev. A: At., Mol., Opt. Phys.* **1992**, *45*, 2641−2644.

(18) Chinnery, P. A.; Humphrey, V. F. Experimental visualization of acoustic resonances within a stadium-shaped cavity. *Phys. Rev. E: Stat. Phys., Plasmas, Fluids, Relat. Interdiscip. Top.* **1996**, *53*, 272−276.

(19) Stein, J.; Stöckmann, H. J. Experimental determination of billiard wave functions. *Phys. Rev. Lett.* **1992**, *68*, 2867−2870.

(20) Sridhar, S. Experimental observation of scarred eigenfunctions of chaotic microwave cavities. *Phys. Rev. Lett.* **1991**, *67*, 785−788.

(21) Arcos, E.; Báez, G.; Cuatláyol, P. A.; Prian, M. L. H.; Méndez-Sánchez, R. A.; Hernández-Saldaña, H. Vibrating soap films: An analog for quantum chaos on billiards. *Am. J. Phys.* **1998**, *66*, 601−607.

(22) Lai, Y.-C.; Xu, H.-Y.; Huang, L.; Grebogi, C. Relativistic quantum chaos—An emergent interdisciplinary field, Chaos: An Interdisciplinary. *Chaos* **2018**, *28*, 052101.

(23) Huang, L.; Lai, Y.-C.; Ferry, D. K.; Goodnick, S. M.; Akis, R. Relativistic quantum scars. *Phys. Rev. Lett.* **2009**, *103*, 054101.

(24) Wong, D.; Velasco, J., Jr.; Ju, L.; Lee, J.; Kahn, S.; Tsai, H. Z.; Germany, C.; Taniguchi, T.; Watanabe, K.; Zettl, A.; Wang, F.; Crommie, M. F. Characterization and manipulation of individual defects in insulating hexagonal boron nitride using scanning tunnelling microscopy. *Nat. Nanotechnol.* **2015**, *10*, 949−U192.

(25) Quezada-López, E. A.; Ge, Z.; Taniguchi, T.; Watanabe, K.; Joucken, F.; Velasco, J. Comprehensive Electrostatic Modeling of Exposed Quantum Dots in Graphene/Hexagonal Boron Nitride Heterostructures. *Nanomaterials* **2020**, *10*, 1154.

(26) Katsnelson, M. I.; Novoselov, K. S.; Geim, A. K. Chiral tunnelling and the Klein paradox in graphene. *Nat. Phys.* **2006**, *2*, 620−625.

(27) Berggren, K. F.; Ji, Z. L. Quantum chaos in nano-sized billiards in layered two-dimensional semiconductor structures, Chaos: An Interdisciplinary. *Chaos* **1996**, *6*, 543−553.

(28) Stöckmann, H.-J. *Quantum Chaos: An Introduction*; Cambridge University Press: 1999.

(29) Nam, S.-G.; Ki, D.-K.; Park, J. W.; Kim, Y.; Kim, J. S.; Lee, H.-J. Ballistic transport of graphene pnp junctions with embedded local gates. *Nanotechnology* **2011**, *22*, 415203.

(30) Zhou, X.; Kerelsky, A.; Elahi, M. M.; Wang, D.; Habib, K. M. M.; Sajjad, R. N.; Agnihotri, P.; Lee, J. U.; Ghosh, A. W.; Ross, F. M.; Pasupathy, A. N. Atomic-Scale Characterization of Graphene p−n Junctions for Electron-Optical Applications. *ACS Nano* **2019**, *13*, 2558−2566.

https://doi.org/10.1021/acs.nanolett.1c02271
Nano Lett. 2021, 21, 8993−8998